

# Modeling and Analysis of Variable-Length Optical Fiber in Air Release

Minghang Li<sup>1</sup>, Yaohui Xue<sup>1</sup>, Zhuo Zhang<sup>1,\*</sup>, Jingze Lv<sup>2</sup>, Feng Tang<sup>1</sup>, Dashan Niu<sup>1</sup> and Jiaxin Wang<sup>1</sup>

<sup>1</sup> Xi'an Modern Control Technology Research Institute, Xi'an 710065, Shaanxi, China

<sup>2</sup> Xidian University, Xi'an 710065, Shaanxi, China

\*Corresponding author: ShanxiZhangz@163.com

**Abstract.** In this paper, the release process of flexible optical fiber from the spool dispenser is studied. In general, the method of adding elements is used to solve the variable-length problem of the flexible optical fiber. However, when this method is applied to optic fiber release with large length, it will cause large computation and difficult convergence. In this paper, the method of power function polynomial fitting of optic fiber posture function and length normalization is used to establish the optic fiber release model. Galerkin method is used to simplify the partial differential equations into differential equations and solve them. To verify the correctness of the theoretical calculation, a test was carried out using an unmanned aerial vehicle carrying a miniature. According to the state of UAV, the shape, falling track and tension distribution of the optical fiber in the air are calculated. The test value of the ground end tension is compared with the theoretical calculation value. The change trend of the two is basically consistent, and the biggest difference is 12.7%. The reasonableness of the modeling and numerical solution method is proved by the above experiment, which provides a method for solving the variable length release problem of large length, low linear density, and slowly changing shape, performing good convergence. This method provides a reference for failure analysis, fault recurrence and trajectory optimization of guidance fiber.

**Keywords:** optical fiber; variable-length release; tension distribution; experimental verification

## 1 Introduction

Inertial navigation technique has excellent characteristics such as anti-interference, large bandwidth, low delay and low bit error rate [1]. Therefore, the use of optical fiber as a communication medium for UAVs and ground control stations can effectively resist electromagnetic interference, and has the advantages of large transmission bandwidth and low delay. Therefore, the use of UAV using optical fiber as a transmission medium received attention from all countries, and multiple types of fiber-optic navigation UAV have been developed base on this technology [2].

The optical fiber is generally wound on the spool in an orderly manner to form a "spool dispenser", which is installed at the bottom of fiber-optic navigation UAV. As UAV flies, the optical fiber is unwound from spool and released into the air [3-5]. The unwinding motion of optical fiber from the spool dispenser as shown in Fig. 1. Since the optical fiber is the only transmission medium for command and image signals, once the optical fiber is broken, the UAV will lose control [6]. Therefore, the motion posture and tension of optical fiber is the key to analyze the release of weak links and failure forms, which is of great significance to the reliability of the UAV.

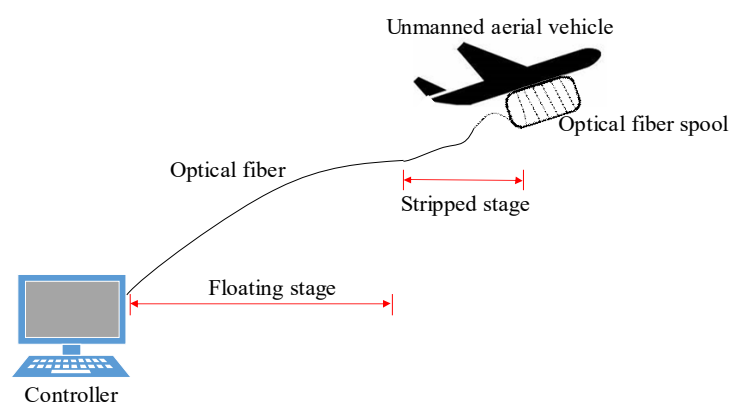


**Fig. 1.** Diagram of fiber-optic navigation UAV.

The optical fiber can be divided into two motion stages after it is unwound from spool dispenser. In the first stage called stripped stage, the optical fiber is stripped from spool dispenser, violently rubbed against the surface of spool dispenser and released in the form of a helix. In the second stage called floating stage, the motion of optical fiber gradually tends to be stable in the air, and the optical fiber shows a quasi-static state. In the first stage, the optical fiber is subjected to the comprehensive influence of tensile, bending, torsion, friction and other loads in a short period of time, which is prone to stress concentration, resulting in optical fiber breakage. In the second stage, the optical fiber is affected by gravity, tension, wind resistance and maneuverable trajectory of the UAV. It is easy to appear that the load exceeds the breaking strength of the optical fiber, resulting in breakage [7].

The analysis of optical fiber in the first stage has been well studied. The earliest fiber release analysis came from the spinning industry, where Padfield [8] conducted a pioneering study on the release posture of yarn from a spool. Fraser [9] and Stanislav [10] analyzed the motion considering friction of yarn on spool according to Padfield's paper. Kothari and Leaf [11] analyzed the influence of different spool shapes on yarn unwinding posture, and also considered factors such as gravity and air resistance. With the development of the study of fiber unwinding motion, there are some advances in the unwinding motion and force of optical fiber from spool dispenser. Lee [12] used Hamilton's principle to analyze the unwinding posture of optical fiber from inner and outer spool dispenser. Based on Lee's research, Kim [13,14] focused on the underwater motion of optical fiber release from spool dispenser, and verified it under low-speed release. Park and Jang [15,16] updated and solved the dynamic equation for optical fiber under variable speed release. Kang et al. and Ren et al. [17,18] established an experi-

mental platform to simulate the release of optical fiber. Li et al. [19] analyzed the unwinding motion of optical fiber in the "quasi-steady state" condition. Wang Rong [20] fitted the bending deformation in optical fiber release.

However, there are few researches on the motion posture of optical fiber in the second stage. The main problem is that the length of released fiber is increasing, which brings some difficulties to analysis. In the similar variable length release analysis problem, Guo [21] proposed a dynamic model of variable-length flexible beams based on absolute node coordinate formulation method. Pang [22] adopted the concentrated mass method to establish the dynamic model of the submarine cable system. Cai Shenglong[23] used the absolute nodal coordinate formulation to derive the dynamic model of a variable length tethered satellite. Zhou et al. [24] established the three-dimensional dynamic equation for the submarine cables, and studied the dynamic response of submarine cables under different working conditions. Feng Shuiliang [25] built a mechanical model of the tethered satellite system based on Lagrange equation, considered tethered elasticity and damping, and conducted a dynamic analysis of the release stage, but did not consider the mass effect of the cable.

The above research mainly use the method of adding or reducing elements to simulate the release and recovery of the cable. However, this method is not suitable for posture analysis of optical fiber. Firstly, the length of optical fiber varies from hundred meters to more than ten kilometers, and the large length will lead to a sharp increase number of element, affecting the computational efficiency. Secondly, the initial state of added element generally is static or equal to aircraft velocity. However, the released cable particle velocity in reality is complicated. Considering the high speed release and small linear density of optical fiber, the inaccurate initial state of added element will lead disturbance to dynamics equation and cause it to diverge. Therefore, there are few studies and reports on force and posture analysis of large length, low linear density and slow changing shape in release process. In this paper, according to the relatively stable posture of optical fiber, power function polynomial is used to fit its posture function, and optical fiber is normalized to solve the variable length problem. Galerkin method is used to transform the partial differential equations into differential equations, and the dynamic equations of the air motion posture of optical fiber are solved numerically. The motion posture of optical fiber, the trajectory of the fiber element and the overall tension distribution along the length direction are analyzed. In order to verify the rationality of the theoretical analysis, a test was carried out using an UAV carrying a miniature. The optical fiber test tension at ground is in good agreement with those of theoretical analysis. The correctness of dynamic equation, boundary condition and solution method are verified and the method adopted in this paper performs good convergence.

## 2 Transient-State Motion Equation of Optical Fiber

### 2.1 Optical Fiber Tension Analysis

In release process, the optical fiber is influenced by tension, gravity, air resistance and damping force. Firstly, the magnitude and direction of tension along optical fiber are

analyzed. Because the bending and torsional stiffness of optical fiber are small, in order to simplify the problem analysis and calculation, only the tensile effect of optical fiber is considered, and the stress changes caused by bending and torsional fiber are ignored. Therefore, the optical fiber has a homogeneous structure in the stretching direction, and its equivalent elastic modulus is  $E$  and cross-sectional area is  $S$ . Let  $s$  denote the unstretched arc length of the optical which varies from 0 to  $L$  and  $p$  refers to the arc length of the optical fiber in the current configuration. For any optical fiber particle, the unstretched length is denoted as  $ds$  and stretched length is denoted as  $dp$ . According to Hooke's law and the definition of engineering strain, the tension of optical fiber is expressed as Eq. (1).

$$T = ES \frac{\Delta l}{l} = ES \left( \frac{dp}{ds} - 1 \right) \quad (1)$$

The coordinate  $OXYZ$  is set on the ground, the  $Z$  axis points to the sky, and the position of optical fiber particle in space can be written as  $\mathbf{R}(s,t)=[x(s,t),y(s,t),z(s,t)]$ .  $\partial x/\partial p$ ,  $\partial y/\partial p$  and  $\partial z/\partial p$  respectively represent the cosine between the tangent vector of stretched optical fiber and the  $x$ ,  $y$ ,  $z$  axes. The relationship of  $\partial x/\partial p$ ,  $\partial y/\partial p$  and  $\partial z/\partial p$  can be written as Eq. (2).

$$\left( \frac{\partial x}{\partial p} \right)^2 + \left( \frac{\partial y}{\partial p} \right)^2 + \left( \frac{\partial z}{\partial p} \right)^2 = \left| \frac{\partial \mathbf{R}}{\partial p} \right|^2 = 1 \quad (2)$$

According to the chain rule, the relationship between unstretched arc length  $s$  and stretched arc length  $p$  is as follows:

$$\frac{\partial \mathbf{R}}{\partial p} = \frac{\partial \mathbf{R}}{\partial s} \frac{ds}{dp} \quad (3)$$

$$\frac{\partial \mathbf{R}}{\partial p} \cdot \frac{\partial \mathbf{R}}{\partial p} = \frac{\partial \mathbf{R}}{\partial s} \cdot \frac{\partial \mathbf{R}}{\partial s} \left( \frac{ds}{dp} \right)^2 = 1 \quad (4)$$

So, the value of  $dp/ds$  is:

$$\frac{dp}{ds} = \left| \frac{\partial \mathbf{R}}{\partial s} \right| \quad (5)$$

By bringing Eq. (5) into Eq. (1), the tension value of optical fiber can be expressed as:

$$T = ES \left( \left| \frac{\partial \mathbf{R}}{\partial s} \right| - 1 \right) \quad (6)$$

Since the tangent vector of stretched optical fiber is  $\partial\mathbf{R}/\partial p$ , the tension of optical fiber can be expressed as:

$$\mathbf{T} = T \frac{\partial\mathbf{R}}{\partial p} = T \frac{\partial\mathbf{R}}{\partial s} \frac{ds}{dp} = ES \left( \left| \frac{\partial\mathbf{R}}{\partial s} \right| - 1 \right) \frac{\partial\mathbf{R}}{\partial s} / \left| \frac{\partial\mathbf{R}}{\partial s} \right| \quad (7)$$

## 2.2 Air resistance Analysis

In release process, the optical fiber will fall slowly under gravity. During the falling process, the optical fiber moves relative to the air, forming air resistance. Secondly, the air resistance received by optical fiber is analyzed. It is observed in experiment that the falling speed of optical fiber is small. According to the principle of fluid mechanics, the air resistance of optical fiber is directly proportional to the square of its normal moving speed and the cross-sectional area of optical fiber along the length direction. The direction of air resistance is opposite to the direction of normal moving velocity. The force of the optical fiber in the air can be shown in Fig. 2.

The velocity of optical fiber particle is assumed as  $\mathbf{v}$ , and the tangential velocity along the tangential direction of optical fiber posture is set as  $\mathbf{v}_t$ . According to the vector algorithm, the normal velocity  $\mathbf{v}_n$  can be calculated as Eq. (8).

$$\begin{aligned} \mathbf{v}_n &= \mathbf{v} - \mathbf{v}_t \\ &= \frac{\partial\mathbf{R}}{\partial t} - \left( \frac{\partial\mathbf{R}}{\partial t} \cdot \frac{\partial\mathbf{R}}{\partial p} \right) \cdot \frac{\partial\mathbf{R}}{\partial p} \\ &= \frac{\partial\mathbf{R}}{\partial t} - \frac{\partial\mathbf{R}}{\partial t} \cdot \frac{\partial\mathbf{R}}{\partial s} \cdot \frac{ds}{dp} \cdot \frac{\partial\mathbf{R}}{\partial s} \cdot \frac{ds}{dp} \\ &= \frac{\partial\mathbf{R}}{\partial t} - \left( \frac{\partial\mathbf{R}}{\partial t} \cdot \frac{\partial\mathbf{R}}{\partial s} \cdot \frac{\partial\mathbf{R}}{\partial s} \right) / \left| \frac{\partial\mathbf{R}}{\partial s} \right|^2 \end{aligned} \quad (8)$$

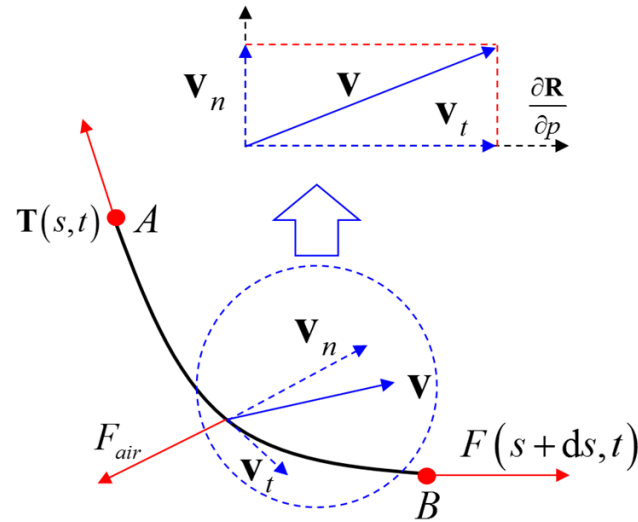


**Fig. 2.** Air resistance diagram of optical fiber.

The projected area  $dS$  of optical fiber in the normal motion direction is shown in Eq.(9).

$$dS = d \cdot ds \quad (9)$$

Where:  $d$  is the diameter of optical fiber. The air resistance of any optical fiber particle  $dp$  is calculated as Eq.(10).

$$\mathbf{F}_{air} = -\frac{1}{2} C \rho_{air} d \cdot ds \cdot |\mathbf{v}_n| \mathbf{v}_n \quad (10)$$

Where:  $C$  is the scale coefficient, obtained by searching the data according to optical fiber normal motion speed  $\mathbf{v}_n$ , and  $\rho_{air}$  is air density.

Therefore, the dynamics equation of optical fiber particle can be written as Eq. (11).

$$\rho \frac{\partial^2 \mathbf{R}}{\partial t^2} ds = \mathbf{T}(s+ds, t) - \mathbf{T}(s, t) - \frac{1}{2} C \rho_{air} d \cdot ds \cdot |\mathbf{v}_n| \mathbf{v}_n - \rho \mathbf{g} \cdot ds \quad (11)$$

Where:  $\mathbf{g}$  is the gravitational acceleration vector and  $\rho$  is the linear density of optical fiber.

The tension  $\mathbf{T}$  can be transformed as follows:

$$\lim_{ds \rightarrow 0} \left[ \frac{\mathbf{T}(s+ds, t) - \mathbf{T}(s, t)}{ds} \right] = \frac{\partial \mathbf{T}(s, t)}{\partial s} \quad (12)$$

Therefore, Eq. (11) can be simplified as:

$$\rho \frac{\partial^2 \mathbf{R}}{\partial t^2} = \frac{\partial \mathbf{T}}{\partial s} - \frac{1}{2} C \rho_{air} d \cdot |\mathbf{v}_n| \mathbf{v}_n - \rho \mathbf{g} \quad (13)$$

### 2.3 Boundary Condition Analysis

When fiber-optic navigation UAV is used, the optical fiber is stored in the bottom of the UAV, and the optical fiber is connected with the ground control platform to build a two-way communication link. According to the application scenario, the spatial position of the optical fiber connected to the ground platform is assumed as  $\mathbf{R}_0(t) = [X_0(t), Y_0(t), Z_0(t)]$ . The position of the optical fiber release point at the bottom of UAV is assumed as  $\mathbf{R}_1(t) = [X_1(t), Y_1(t), Z_1(t)]$ . Since the optical fiber is gradually released and its length changes with time, which is denoted as  $L(t)$ . The optical fiber flight and boundary conditions are shown in Fig. 3.

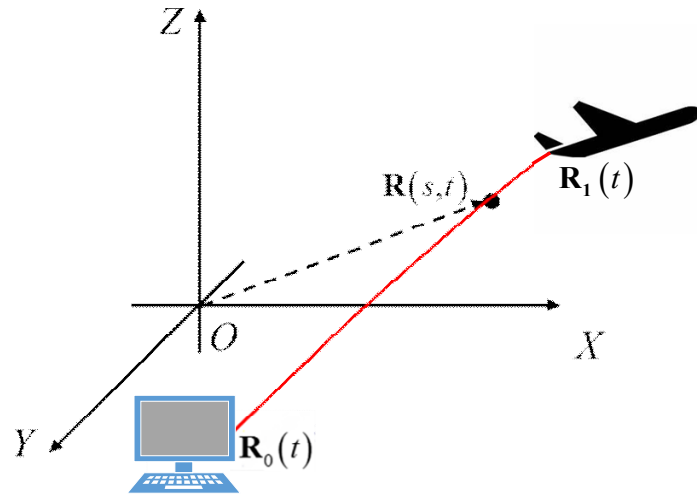


**Fig. 3.** Optical fiber flight and boundary conditions.

Therefore, the boundary conditions of optical fiber at the ground endpoint and the release endpoint are shown as Eq.(14).

$$\begin{cases} \mathbf{R}(0, t) = \mathbf{R}_0(t) \\ \mathbf{R}(L(t), t) = \mathbf{R}_1(t) \end{cases} \quad (14)$$

Since the length of released optical fiber varies with time, a set of governing equations is needed to describe the variational length of optical fiber. According to the characteristics of optical fiber release process, the acceleration, speed and length of optical fiber release are equal to the flight acceleration, speed and trajectory length of the aircraft. The governing equation of fiber length variation law can be obtained as follows:

$$\left\{ \begin{array}{l} \frac{d^2 L(t)}{dt^2} = \sqrt{\left(\frac{d^2 X_1}{dt}\right)^2 + \left(\frac{d^2 Y_1}{dt}\right)^2 + \left(\frac{d^2 Z_1}{dt}\right)^2} \\ \frac{dL(t + \Delta t)}{dt} \approx \frac{dL(t)}{dt} + \Delta t \frac{d^2 L(t)}{dt^2} \\ L(t + \Delta t) \approx L(t) + \Delta t \frac{dL(t)}{dt} + \frac{1}{2} \Delta t^2 \frac{d^2 L(t)}{dt^2} \end{array} \right. \quad (15)$$

### 3 Numerical Solution Method

The length of released optical fiber changes with time and the solution domain of Eq. (13) changes with time. In order to solve this problem, firstly, the optical fiber is normalized in the length direction. Secondly, the motion posture function of optical fiber in the air is fitted with a power function polynomial. Thirdly, Galerkin method is used to solve the coefficients of the power function [26]. The boundary conditions are also time-varying, the assumed posture function of optical fiber should be homogenized to

construct a suitable basis function. The position function of any point on the released optical fiber is assumed as Eq. (15).

$$\begin{cases} x(s,t) = \varphi_x(s,t) + u(s,t) \\ y(s,t) = \varphi_y(s,t) + v(s,t) \\ z(s,t) = \varphi_z(s,t) + w(s,t) \end{cases} \quad (16)$$

Where:

$$\begin{cases} \varphi_x(s,t) = \frac{(X_1(t) - X_0(t))}{L(t)} s + X_0(t) \\ \varphi_y(s,t) = \frac{(Y_1(t) - Y_0(t))}{L(t)} s + Y_0(t) \\ \varphi_z(s,t) = \frac{(Z_1(t) - Z_0(t))}{L(t)} s + Z_0(t) \end{cases} \quad (17)$$

The function  $\varphi_x(s,t)$ ,  $\varphi_y(s,t)$  and  $\varphi_z(s,t)$  satisfies exactly the boundary conditions of Eq.(14), so the boundary condition of function  $u(s,t)$ ,  $v(s,t)$  and  $w(s,t)$  can be re-written as:

$$\begin{cases} u(0,t) = 0 & u(L(t),t) = 0 \\ v(0,t) = 0 & v(L(t),t) = 0 \\ w(0,t) = 0 & w(L(t),t) = 0 \end{cases} \quad (18)$$

According to Galerkin method and the boundary conditions shown in Eq(18), using the power function as the base function to construct the approximate solution  $u(s,t)$ ,  $v(s,t)$  and  $w(s,t)$  are written as:

$$\begin{cases} u(s,t) = \sum_{i=1}^n a_i(t) \left(1 - \frac{s}{L(t)}\right) \left(\frac{s}{L(t)}\right)^i \\ v(s,t) = \sum_{i=1}^n b_i(t) \left(1 - \frac{s}{L(t)}\right) \left(\frac{s}{L(t)}\right)^i \\ w(s,t) = \sum_{i=1}^n c_i(t) \left(1 - \frac{s}{L(t)}\right) \left(\frac{s}{L(t)}\right)^i \end{cases} \quad (19)$$

In the power function construction in Eq.(17) and Eq. (19),  $s/L(t)$  term is used to achieve normalization, so that the posture function changes within the interval of [0,1].

This analysis method does not care about the initial state of released optical fiber element, and does not need to add new element, but only analyzes the posture function of optical fiber.

Bringing the Eq. (16), Eq. (17) and Eq. (19) into Eq. (13), both sides of Eq. (13) are multiplied by the basis function. The variable  $s$  of Eq. (13) is integrated over the interval 0 to  $L(t)$ . Make the integral value of Eq. (13) equal to zero, resulting in  $3n$  equations, the specific form is as follows:

$$\int_0^{L(t)} \left( \left( \rho \frac{\partial^2 \mathbf{R}}{\partial t^2} - \frac{\partial \mathbf{T}}{\partial s} - \frac{1}{2} C \rho_{air} d \cdot |\mathbf{v}_n| \mathbf{v}_n - \rho \mathbf{g} \right) \cdot \left( 1 - \frac{s}{L(t)} \right) \left( \frac{s}{L(t)} \right)^{i=1 \sim n} \right) ds = \mathbf{0} \quad (20)$$

When the initial posture of optical fiber is determined, that is,  $a_i(0)$ ,  $da_i(0)/dt$ ,  $b_i(0)$ ,  $db_i(0)/dt$ ,  $c_i(0)$  and  $dc_i(0)/dt$  is known, then the unknown terms  $d^2a_i(0)/dt^2$ ,  $d^2b_i(0)/dt^2$  and  $d^2c_i(0)/dt^2$  in Eq.(20) can be calculated. The coefficient calculation of the power function is shown in Eq.(21) and Eq.(22).

$$\begin{cases} \frac{da_i(t + \Delta t)}{dt} \approx \frac{da_i(t)}{dt} + \Delta t \frac{d^2a_i(t)}{dt^2} \\ \frac{db_i(t + \Delta t)}{dt} \approx \frac{db_i(t)}{dt} + \Delta t \frac{d^2b_i(t)}{dt^2} \\ \frac{dc_i(t + \Delta t)}{dt} \approx \frac{dc_i(t)}{dt} + \Delta t \frac{d^2c_i(t)}{dt^2} \end{cases} \quad (21)$$

$$\begin{cases} a_i(t + \Delta t) \approx a_i(t) + \Delta t \frac{da_i(t)}{dt} + \Delta t^2 \frac{d^2a_i(t)}{dt^2} \\ b_i(t + \Delta t) \approx b_i(t) + \Delta t \frac{db_i(t)}{dt} + \Delta t^2 \frac{d^2b_i(t)}{dt^2} \\ c_i(t + \Delta t) \approx c_i(t) + \Delta t \frac{dc_i(t)}{dt} + \Delta t^2 \frac{d^2c_i(t)}{dt^2} \end{cases} \quad (22)$$

#### 4 Calaulation Results and Experimental Verification

In order to verify the rationality of theoretical analysis, an experimental verification is built to test the optical fiber release process. The construction of the experimental system is shown in Fig. 4. The experimental scheme is as follows: a miniature of optical fiber spool dispenser is made, and it is installed on the UAV, and the other endpoint of the optical fiber is fixed on the force sensor on the ground, as shown in Fig. 5. The test tool is used to wrap the optical fiber in a ring, and one end of the ring is connected to a tension sensor to measure the tension of the optical fiber. The UAV flies according to

the preset trajectory and speed, the highest speed is about 180m/s, the whole flight process lasts about 26.5s.

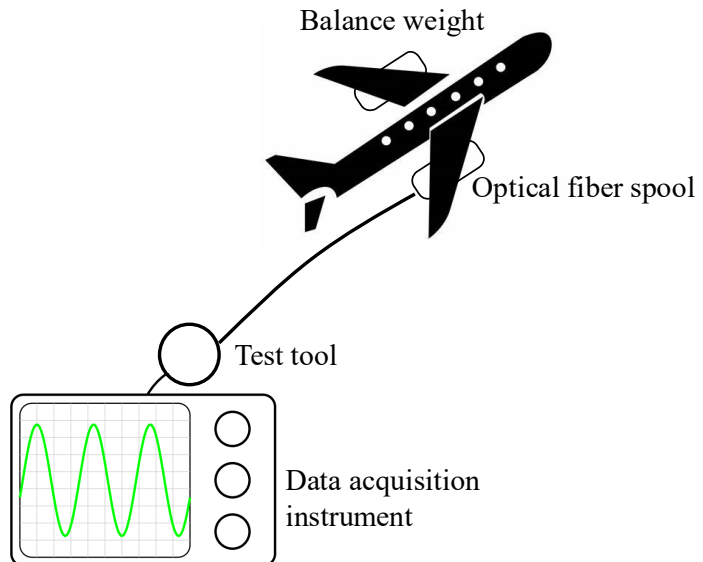


**Fig. 4.** Test system construction diagram.

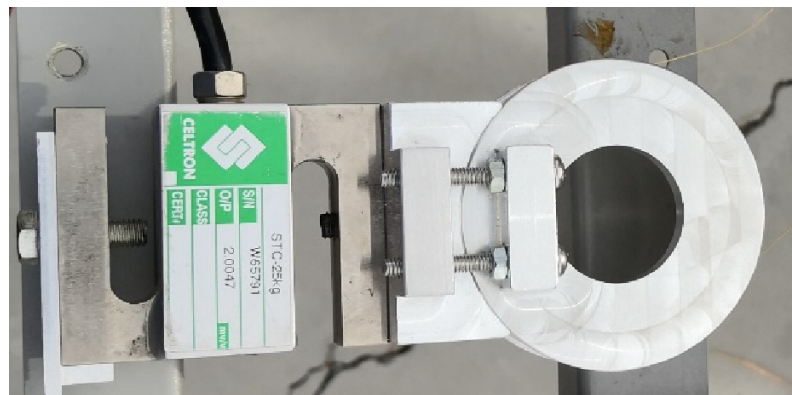


**Fig. 5.** Test tool.

In order to balance calculation efficiency and accuracy,  $n=5$  is used in theoretical calculation, and a total of 15 unknowns in  $X$ ,  $Y$  and  $Z$  directions can be solved. Fig. 6 shows the release posture of optical fiber at different times, where the blue dots represent the preset flight trajectory of UAV and the black line represents the release posture of optical fiber. It is shown that, the released optical fiber slowly drops in the air, but is always tensioned and the posture is relatively stable. Fig. 7, Fig. 8 and Fig. 9 show the trajectory of the released optical fiber particle in the air at 10s, 15s and 25s, and the speed variation of  $X$  and  $Y$  with time. It can be seen from these three figures that: 1. The initial speed of the fiber particles released at different times is different, and they are not static 2. The speed of the fiber particles at different times eventually tends to be stable, and the horizontal speed tends to be 0, and the vertical speed tends to be -1m/s. These phenomena show that the boundary conditions of the released fiber change with time, and do not simply fall gradually from the static state.

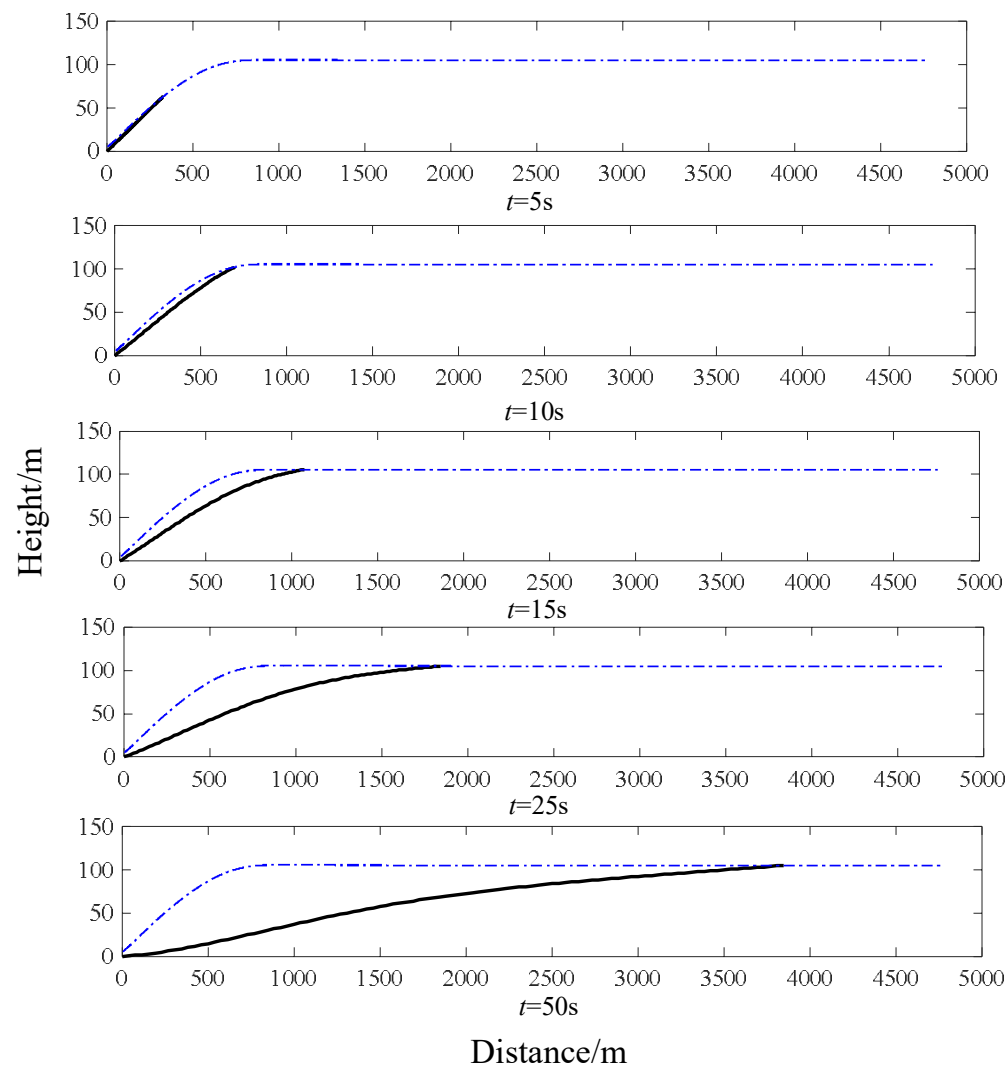
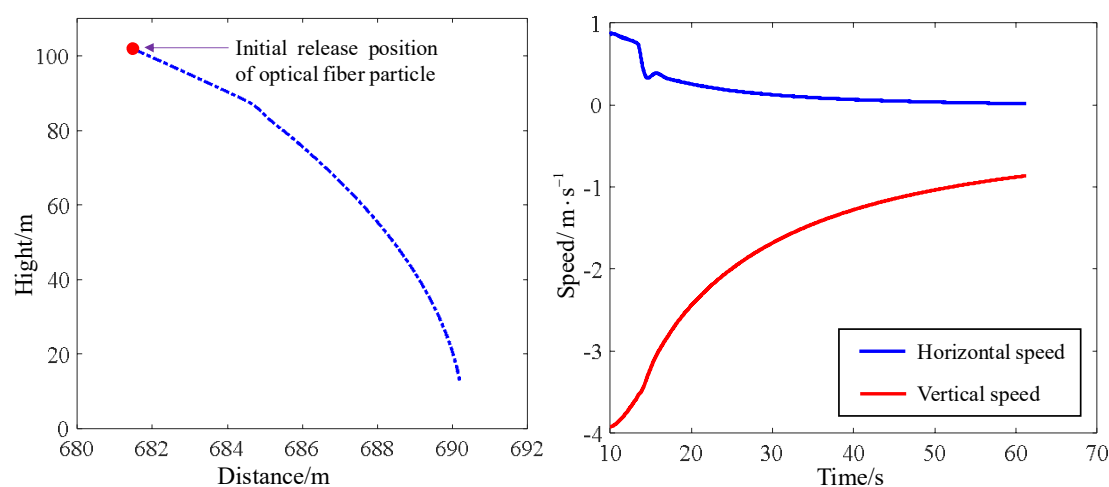
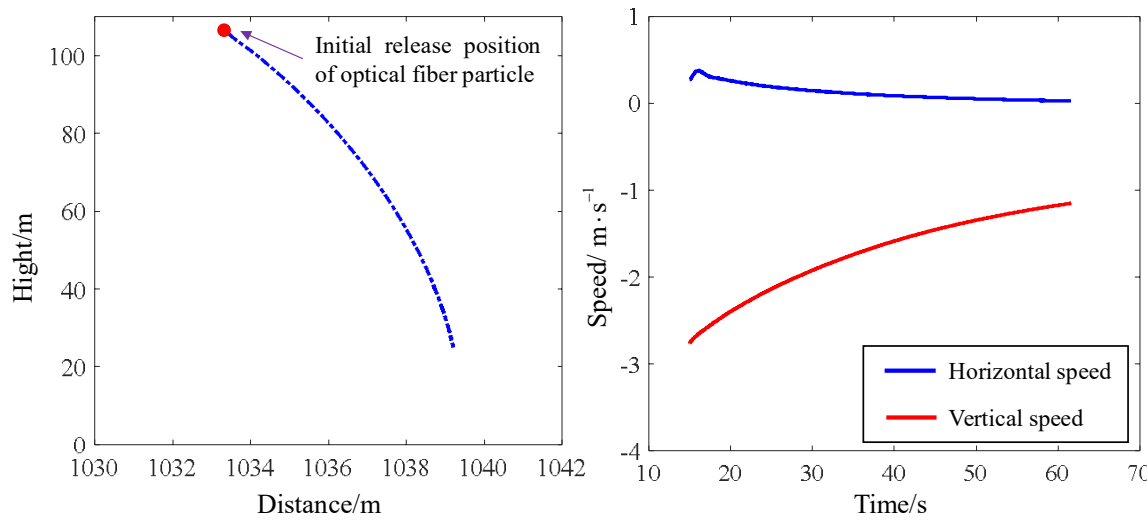


**Fig. 6.** Posture of optical fibers in air at different times (Ratio of vertical data to horizontal data is 5:1).



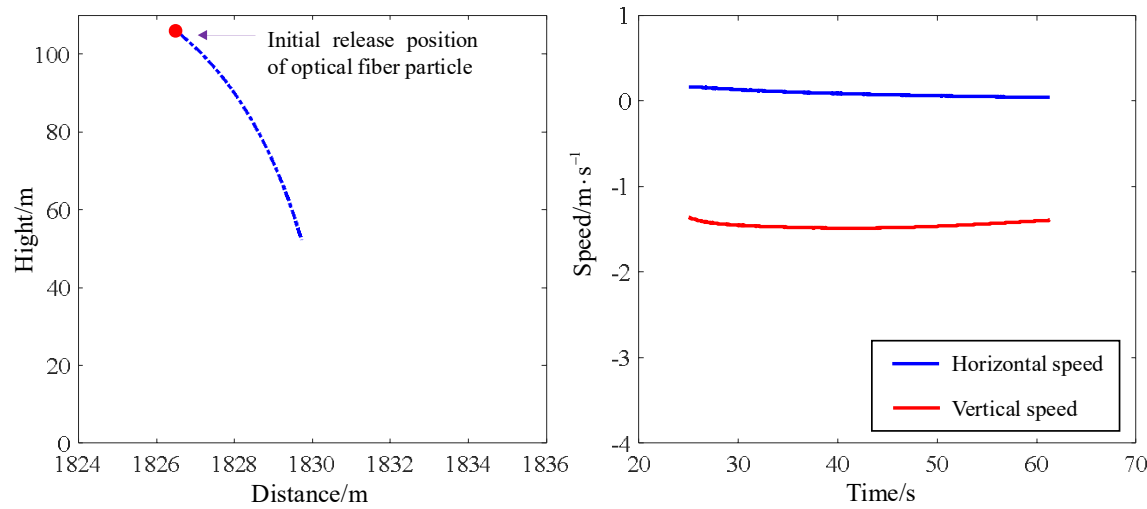
(a) Optical fiber microelement in the air falling trajectory (b) Variation of motion velocity of optical fiber particle

**Fig. 7.** Trajectory and velocity change of the fiber particles released at 10s in air.



(a) Optical fiber microelement in the air falling trajectory (b) Variation of motion velocity of optical fiber particle

**Fig. 8.** Trajectory and velocity change of the fiber particles released at 15s in air.



(a) Optical fiber microelement in the air falling trajectory (b) Variation of motion velocity of optical fiber particle

**Fig. 9.** Trajectory and velocity change of the fiber particles released at 25s in air.

According to Eq. (17) and Eq. (19), the optical fiber particle velocity at released point can be expressed as Eq. (23).

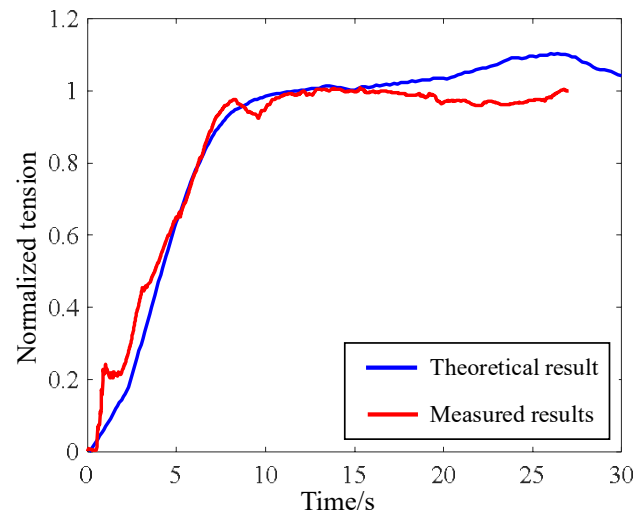
$$\begin{cases} \frac{dx(L,t)}{dt} = \frac{1}{L} \frac{dX_1}{dt} - \frac{X_1}{L^2} \frac{dL}{dt} \\ \frac{dy(L,t)}{dt} = \frac{1}{L} \frac{dY_1}{dt} - \frac{Y_1}{L^2} \frac{dL}{dt} \\ \frac{dz(L,t)}{dt} = \frac{1}{L} \frac{dZ_1}{dt} - \frac{Z_1}{L^2} \frac{dL}{dt} \end{cases} \quad (23)$$

Eq. (23) shows that the optical fiber particle velocity at released point is affected by three factors: the aircraft velocity, the aircraft position and the released optical fiber length in the air. When the optical fiber is just released from the aircraft, it has an initial

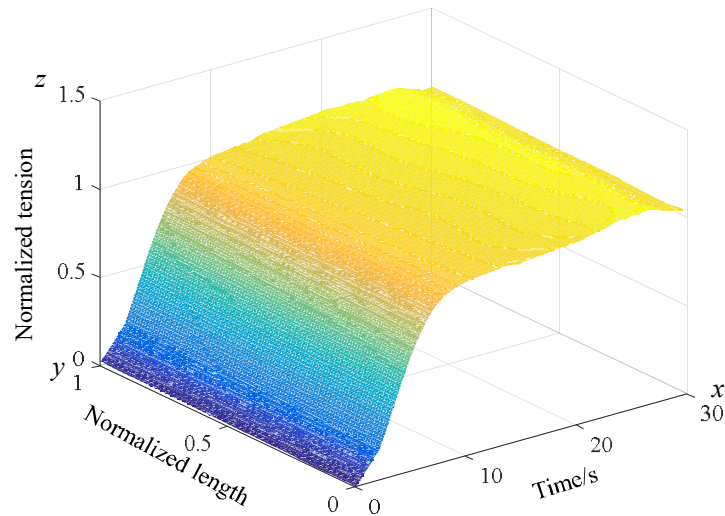
velocity, but the initial speed is much less than the aircraft speed. In horizontal direction, it will continue to move some distance along with the flight direction, and in the vertical direction, it will slowly fall over time. However, after the optical fiber particle is released in the air, its velocity gradually decreases and eventually tends to be zero. As the flight distance of the aircraft increases, the initial speed of optical fiber particle velocity at released point also decreases and eventually tends to be zero. So the released optical fiber has been "floating" in the air and does not fall on the ground.

Fig. 10 compares the theoretical optical fiber tension at the ground endpoint with the measured results after noise reduction. In this figure, the experimental result at 26.5s is taken as the benchmark. The theoretical result and the measured result are normalized by this benchmark. As shown in Fig.9, the measured tension increases first and then gradually stabilized with time. This is because the aircraft accelerated from a standstill, resulting in increasing tension on optical fiber. After the aircraft levelled out, the speed and direction of aircraft were relatively stable, and the tension of optical fiber also tended to be stable. According to the comparison between theoretical results and measured results, it can be seen that in the tension growth stage, the two are in good agreement. In the tension stabilization stage, there were some fluctuations in theoretical tension, and the largest difference in tension appeared at about 24.8s, with a difference of about 12.7%.

Fig. 11 shows the theoretical tension distribution on the fiber at different times, where the X-axis represents the time, the Y-axis represents the normalized optical fiber length, and the Z-axis represents the normalized magnitude of the tension. In Fig. 10, the measured optical fiber tension at the ground endpoint at 26.5s is taken as the benchmark of Z-axis. As can be seen from Fig. 11, observing along the X-axis, the tension along optical fiber rises rapidly in the initial acceleration stage. When the aircraft levelled out, the tension along optical fiber is basically stable. Observing along the Y-axis, the internal tension of optical fiber fluctuates slightly, and the tension of ground endpoint and released endpoint is close.



**Fig. 10.** Comparison between the measured value and the theoretical value of the ground endpoint fiber tension.



**Fig. 11.** Variation of theoretical tension distribution of optical fiber with time.

## 5 Summary

In this paper, according to the characteristics of released optical fiber movement in the air, polynomial power function is used to fit its posture function. Considering the optical fiber length in the air changes with time, the dynamic equation is solved by normalization and Galerkin method, and the posture and tension distribution of optical fiber are calculated at different times. It is found that:

- 1) When the optical fiber particle is released from the aircraft, its speed is neither zero nor equal to the speed of the aircraft, and its initial speed is affected by three factors: the speed of the aircraft, the position and the length of the guidance fiber in the air. The released optical fiber particle moves slowly in the horizontal direction, and fall slowly to the ground in the vertical direction.
- 2) The tension on released optical fiber always exists, and the entire optical fiber is always in the air and will not fall on the ground.
- 3) The optical fiber tension rises rapidly in the initial acceleration stage of aircraft, and when the aircraft levels out, the tension on the fiber is basically stable.
- 4) The internal tension of optical fiber fluctuates slightly, and the tension of ground endpoint and released endpoint is close.
- 5) In order to verify the rationality of theoretical analysis, the UAV was used to carry a miniature of optical fiber spool. In the experiment, the ground endpoint tension of the optical fiber is measured and compared with the theoretical results. It is found that the theoretical results are in good agreement with measured results during the acceleration stage of the aircraft. When the aircraft levelled out, there is a deviation between theoretical results and measured results, the maximum difference is about 12.7%, but the overall trend is basically the same. The main reason is that factors such as the change of wind field and the friction of optical fiber with spool have not been considered during the flight of the UAV. Therefore, in the next research work, it is necessary to study the influence of these factors on the force and shape of the optical fiber.

This paper provides a dynamic equation modeling and solving method for long-length, variable-length, low-density and slow-changing posture fiber release problem. It solves the problems of unknown posture and tension of released optical fiber, and provides reference for failure analysis, fault recurrence and trajectory optimization of aircraft.

## References

1. Yang fan, Wang yudong, Ma baoji and Meng xiaotong. Residual Stress-strain and Numerical Simulation of Deformation on Fiber Optic Cable Package Curing. *Journal of Projectiles, Rockets, Missiles and Guidance*, 2023, 43(02):12-19.
2. Li Zhengmin, Bi Meihua, Zhao Lou, Xu Hangyong, Tneg Xuyang Hu Miao. Performance improvement by an optimum commanding-based Non-Uniform quantization scheme in low-bit resolution IMDD-UFMC system. *Optical Fiber Technology*, 2024, 88, 103820.
3. Qu F. Simulation of winding process of guidance optical fiber. Xi'an: Xi'an Technological University, 2021.
4. Zhu Jianxiong, Yuksek Nuh S, Almasri M and Feng Zaichun. Numerical modeling of dynamic response of miniature multi-impact electromagnetic device for low and wide range frequencies energy harvesting. *Proceedings of the Institution of Mechanical Engineers, Part C: Journal of Mechanical Engineering Science*, 2019, 233(7):2400-2409.
5. Zhu Jianxiong, Lin Jie, Yuksek Nuh S, Almasri M and Feng Zaichun. Dynamic phenomena and analysis of MEMS capacitive power harvester subjected to low-frequency excitations. *Nonlinear Dynamics*, 2015, 79: 673-688.
6. Tang WeiJiang, Liu WeiDong, Gao Zhou, Zhang Kai and Zhao Peidong. Stress distribution and influence factors of fiber-optic coil for unmanned submersible vehicle .*Acta Armamentarii*, 2021, 42(5):1053-1064.
7. Huang Luyao, Xu Yongxin, Jiang Wenqing, Xue Lei, Hu Weisheng, Yi Lilin. Performance and complexity analysis of conventional and deep learning equalizers for the high-speed IMDD PON. *Journal of Lightwave Technology*, 2022, 40(14): 4528-4538.
8. Daphne G. Padfield. The motion and tension of an unwinding thread. I. *Proceedings the Royal Society A*, 1958, 245: 382-407.
9. Fraser W. B., Ghosh T. K. and Batra S. K. On unwinding yarn from a cylindrical package. *Proceedings the Royal Society A*, 1992, 436: 479-498.
10. Stanislav Praček, Nace Pušnik, Barbara Simončič, Barbara Simoncic. Balloon theory of yarn during unwinding from package. *Textile Research Journal*, 2016, 86(14).
11. Kothari V K, Leaf G A V. The unwinding of yarns from package, part III: unwinding from conical packages. *Journal of the Textile Institute Transactions*, 1979, 70: 172-183.
12. Lee Jae-Wook, An Deuk-Man, Yoo Wan-Suk. Derivation of equations of motion of an unwinding cable from a cylindrical spool package. *Journal of Mechanical Science and Technology*, 2011, 25: 1287-1296.
13. Kim Kun-Woo, Lee Jae-Wook, Yoo Wan-Suk. Verification of simulation for unwinding motion of cable in water by physical experiment. *Nonlinear Dynamics*, 2014, 77: 553-568.
14. Kim Kun-Woo, Lee Jae-Wook, Yoo Wan-Suk. Unwinding motion of cable by taking into consideration effect of bending on cable, *International Journal of Non-linear Mechanics*. 2014, 65:107-120.
15. Park Hyun-Gyu, Kang Ji-Heon, Kim Kun-Woo, Lee Jae-Wook, Choi Chang-Young, Jang Jin-seok and Kim Sung-yong. Verification of numerical analysis for unwinding cable with time-varying unwinding velocity. *Textile Research Journal*, 2021, 91(17-18): 1957-1973.

16. Jang Jin-Seok, Kim Kun-Woo, Kang Ji-Heon, Park Hyun-Gyu, Cho Young-Jae, Lee Jae-Wook. Derivation of equations of motion of an unwinding cable considering transient-state tensile force in time-varying unwinding velocity. *Nonlinear Dynamics*, 2020, 100: 3199-3241.
17. Kang Ji-Heon, Kim Kun-Woo, Lee Jae-Wook, Cho Yong-Jae and Jin-Seok Jang. Development of a test method and experimental study on cable unwinding. *Proceedings of the Institution of Mechanical Engineers, Part C: Journal of Mechanical Engineering Science*. 2021, 235(15): 2653-2667.
18. Ren pengyuan and Ma baoji. Design of Measurement and Control System for Optical Fiber Pay-off Device Based on LabVIEW. *Mechanical & Electrical Engineering Technology*, 2023, 52(02):195-200.
19. Li MingHang, Zhang Zhuo, Tang Feng, Xue YaoHui, Wang JiaXin and Niu DaShan. Analysis of Posture and Tension of Guidance Optical Fiber in High Speed Release. *Journal of Projectiles, Rockets, Missiles and Guidance*, 2024, 44(03):1-10+21.
20. Wang Rong, Li Zhenhua, Bian Baomin. Modeling and characteristics analysis of strong bending state of fiber optical cable. *Journal of Air Force Engineering University (Natural Science Edition)*, 2014, 15(2): 71-75.
21. Guo JiaWen. Research on dynamics and energy-preserving numerical algorithm of the variable-length cable and beam with sliding constraints. *Harbin Institute of Technology*, 2023.
22. Pang Shi-kun, Liu Jing-yang, Chen Hong, Wang Jian, Yi Hong. Analysis of motion state of the tow-part underwater towed vehicle system during cable deployment. *Oceans 2017*, Aberdeen, the UK.
23. Cai Shenglong. Deployment and dragging control of tethered satellites based on the variable length cable model. *Harbin: Harbin Institute of Technology* 2019.
24. Zhou Hang, Yan Xue, Hu Dean, and Han Xu. A hamiltonian global nodal position finite element method for dynamics analysis of submarine cables. *Ocean Engineering*, 2022, 266: 112992.
25. Feng Shuiliang. Dynamics and stability for deployment of tethered satellite system. Nanjing: Nanjing University of Aeronautics and Astronautics 2020.
26. Li Dan, Wang Chunwei and Wang Junping. Curved elements in weak Galerkin finite element methods. *Computers & Mathematics with Applications*, 2024, 153: 20-32.